γ-Ray Generation from Plasma Wakefield Resonant Wiggler

Bifeng Lei,[1,2,*] Jingwei Wang,[1,3,†] Vasily Kharin,[1] Matt Zepf,[1,2] and Sergey Rykovanov[1,‡]
[1]Helmholtz-Institut Jena, 07743 Jena, Germany
[2]Faculty of Physics and Astronomy, Friedrich-Schiller-Universität Jena, 07743 Jena, Germany
[3]Shanghai Institute of Optics and Fine Mechanics, Chinese Academy of Sciences, 201800 Shanghai, China

(Received 9 January 2018; published 30 March 2018)

A flexible gamma-ray radiation source based on the resonant laser-plasma wakefield wiggler is proposed. The wiggler is achieved by inducing centroid oscillations of a short laser pulse in a plasma channel. Electrons (self-)injected in such a wakefield experience both oscillations due to the transverse electric fields and energy gain due to the longitudinal electric field. The oscillations are significantly enhanced when the laser pulse centroid oscillations are in resonance with the electron betatron oscillations, extending the radiation spectrum to the gamma-ray range. The polarization of the radiation can be easily controlled by adjusting the injection of the laser pulse into the plasma channel.

DOI: 10.1103/PhysRevLett.120.134801

Laser-plasma-based radiation sources have attracted a solid amount of attention, mostly due to their compactness (centimeter scale) [1–3], as compared to conventional facilities that include electron accelerators and insertion devices, such as magnetic undulators or wigglers. Just like conventional synchrotron facilities, laser-plasma-based sources have a lot of potential for various applications in science and technology [4–7]. Bright ultraviolet and x-ray radiation can be generated by electrons undergoing betatron oscillations in a plasma wakefield excited by an intense short laser pulse propagating in underdense plasmas [3,8–10]. Gamma-ray radiation from the wakefield-based sources can be achieved by enhancing the amplitude of the betatron oscillations when the electrons interact with the rear of the laser pulse [2,11,12], or by inducing the bubble hosing through the carrier envelope phase (CEP) effect of the self-steepened laser pulse [13]. Most of the previous works focused on the nonlinear plasma wakefield regime, which is only accessible with laser pulses with relativistic intensities, i.e., $I > 10^{18}$ W/cm^2 for a micron laser wavelength. Recently, a flexible and narrow-band laser-plasma-based undulator was proposed to generate x-ray radiation with tunable polarization in the linear wakefield regime [14–16]. The undulator field is generated by injecting a laser pulse into a plasma channel off axis and with an angle, or by the beating of a mixture of high-order laser modes. If an electron is properly injected into the wakefield generated by the laser pulse wiggling in the plasma channel, it can undergo forced harmonic oscillations and emit x-ray radiation with kilo-electron-volt photon energies. However, it is hard to further increase the emitted photon energy, which requires a much smaller undulator period ($\ll 1$ mm) or much larger electron energy ($\gg 1$ GeV).

In this Letter, we show that it is possible to significantly increase the energy of emitted photons up to the gamma-ray range in the plasma wiggler based on a linear wakefield by resonating the electron betatron and laser centroid oscillations in the parabolic plasma channel. As schematically demonstrated in Fig. 1, a short laser pulse (depicted with the purple color on the left) is injected into a plasma channel with an initial centroid displacement. The laser pulse, as well as the excited plasma wakefield, will then oscillate with a period of $2\pi Z_R$ while propagating in the plasma channel. Here, Z_R is the laser pulse Rayleigh length. An electron beam following the laser pulse will experience forced undulator oscillations due to the oscillating wakefield and will experience betatron oscillations due to the intrinsic transverse structure of the wakefield. The resonance between

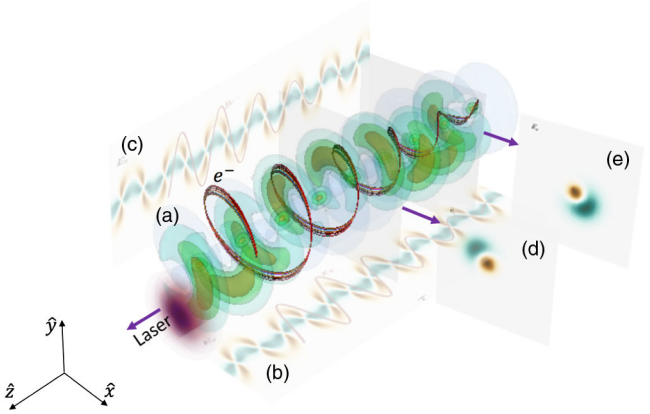

FIG. 1. Demonstration of a resonant plasma wiggler. (a) 3D helical plasma wakefield (colored surface) and short laser pulse (purple spot) on the left. Trajectories of the electron beam are shown by red lines, which linearly increase with time. (b) Projection of the transverse electric field E_x and one electron trajectory on the $\hat{x}\hat{z}$ plane. (c) Projection of the transverse electric field E_x and electron trajectory on the $\hat{y}\hat{z}$ plane. (d,e) Slices of the transverse electric field E_x at two different longitudinal positions z.

these two kinds of oscillations leads to a linear increase of the oscillating amplitude of the injected electron beam, whose trajectories are depicted with the red solid lines in Fig. 1. After some distance, this resonance will die out because of the acceleration of the electron beam in the wakefield. As a result, a semisteady large-amplitude oscillating pattern appears and lasts for a long distance, leading to the generation of high-energy gamma-ray radiation with high brightness.

A laser pulse can be guided in a tailored plasma channel to suppress the pulse diffraction [17–19] and to sustain a large accelerating gradient for a long distance. The radial profile of a plasma channel is parabolically distributed as $n(r') = n_0 + r'^2\Delta n/w_0'^2$, where n_0 is the initial on-axis plasma density, $\Delta n = (\pi r_e' w_0'^2)^{-1}$ is the channel depth, r_e' is the classical electron radius, and w_0' is the initial spot size of the laser pulse in centimeter-gram-second (cgs) units. It has been shown that if a short laser pulse enters such a plasma channel off axis or under an angle, its centroid oscillates according to [14,15,20]

$$\mathbf{r}_c(\tau) = \mathbf{r}_{c0}\cos\Omega\tau + \frac{\boldsymbol{\theta}_{r,0}}{\Omega}\sin\Omega\tau, \tag{1}$$

where $\boldsymbol{r}_{c0} = (x_{c0}, y_{c0})$ is the injection position of the laser pulse and $\boldsymbol{\theta}_{r,0} = (\theta_{x0}, \theta_{y0})$ is the injection angle with respect to the propagation axis, $\Omega = 1/Z_R$ with $Z_R = k_p\pi w_0'^2/\lambda_L$. Note that throughout the Letter, length is normalized by the plasma wave number k_p, e.g., $x = k_p x'$, where $k_p = \sqrt{(4\pi n_0 e^2)/(m_e c^2)}$, m_e is the mass of the electron, and c is the speed of light in vacuum; and time is normalized by the plasma frequency ω_p, e.g., $\tau = \omega_p t'$, where x' and t' are in cgs units. The polarization of the laser centroid oscillation can be controlled by choosing the initial transverse injection positions and angles as seen from Eq. (1). As a result, the same polarization of the radiation can be achieved. For simplicity, here we only focus on the case of linear polarization in the $\hat{x}\,\hat{z}$ plane. Other cases, such as linear polarization in the $\hat{y}\,\hat{z}$ plane or circular polarization, can be treated in the same way. By injecting a short laser pulse into the plasma channel off axis in the $\hat{x}\,\hat{z}$ plane, the linearly polarized centroid oscillation can be expressed as

$$x_c(\tau) = x_{c0}\cos\Omega\tau \quad \text{and} \quad y_c(\tau) = 0. \tag{2}$$

Considering a linearly $\hat{x}$-polarized ($a_y = 0$) Gaussian laser pulse with a moderate strength $a_x = a_0\exp(-\xi^2/w_z^2)\times\exp(-[x - x_c(\tau)]^2/w_m^2)$, where $a_0 < 1$ is the normalized laser intensity, w_z is the initial pulse length, $\xi = k_p(z' - ct') = z - \tau$ is the comoving variable, and $w_m = k_p/\sqrt{\pi r_e'\Delta n}$ is the matched initial pulse spot size [21], the generated wakefield is then given by [15]

$$E_z = a_0^2 C e^{-2[x - x_c(\tau)]^2/w_m^2}\cos(\xi), \tag{3}$$

$$E_x = -\frac{4a_0^2 C}{w_m^2}[x - x_c(\tau)]e^{-2[x - x_c(\tau)]^2/w_m^2}\sin(\xi), \tag{4}$$

where the constant $C = \sqrt{\pi/8e} \simeq 0.38$ for the linearly polarized laser pulse of optimized length $w_z = 2$. The transverse field $E_x(\xi, x, \tau)$ in Eq. (4) creates the wiggler field for the injected electrons.

For a wide laser pulse ($|w_m| \gg |x - x_c|$), the exponential term $\exp[-2(x - x_c)^2/w_m^2] \approx 1$, especially in the early interaction stage. Assuming $\beta_x = dx/d\tau \ll dz/d\tau \approx 1$, and neglecting the $(dx/dt)^2$ term in the momentum equation of the electron, one can get an equation for the transverse motion of an electron in the oscillating wakefield E_x:

$$\frac{d^2x}{d\tau^2} + \frac{R_\delta}{1 + R_\delta\tau}\frac{dx}{d\tau} + \frac{\Omega^2}{\mu(1 + R_\delta\tau)}x = \frac{x_{c0}\Omega^2\cos(\Omega\tau)}{\mu(1 + R_\delta\tau)}, \tag{5}$$

where $\mu = -\mu_0/\sin\xi$ with $\mu_0 = \Omega^2/\Omega_\beta^2$, and $\Omega_\beta = \sqrt{4a_0^2 C/(\gamma_0 w_m^2)}$ is the frequency of betatron oscillation. In Eq. (5), the electron energy gain due to acceleration in the wakefield is described as $\delta = -\int_0^\tau(\beta_x E_x + E_z)d\tau' \simeq R_\delta\tau$. The energy-gain rate is given by $R_\delta = -w_m^2\Omega_\beta^2\cos\xi/4$. It is easy to find that the oscillation occurs in the phase range $-\pi \le \xi \le -\pi/2$. The phase of an injected electron in the wakefield can be approximately locked at a fixed position by employing a longitudinally tapered plasma density [22]. Then, we can treat an electron inside the beam with $\xi \simeq \xi_0$, where ξ_0 is the initial injecting phase of the electron. By defining the new variable $s = (2Q_f/\mu)\sqrt{1 + \tau\Omega/Q_f}$, where $Q_f = \Omega/R_\delta$ is the initial quality factor of the oscillation, the equation of motion Eq. (5) can be rewritten as

$$\frac{d^2x}{ds^2} + \frac{1}{s}\frac{dx}{ds} + x = g(s), \tag{6}$$

where $g(s) = x_{c0}\cos[(\mu/4Q_f)s^2 - Q_f)$. The solution is given by

$$x(s) = [c_1 + \nu_1(s)]J_0(s) + [c_2 + \nu_2(s)]Y_0(s), \tag{7}$$

where $J_0(s)$ and $Y_0(s)$ are the Bessel functions of the first and second kinds, respectively, the constants are given by $c_1 = -(x_0 Y_{10} + u_{x0}Y_{00})/W_0$ and $c_2 = (x_0 J_{10} + u_{x0}J_{00})/W_0$, and the variable coefficients are given by $\nu_1(s) = -\int_{s_0}^s[Y_0(s')g(s')/W(s')]ds'$ and $\nu_2(s) = \int_{s_0}^s[J_0(s')g(s')/W(s')]ds'$. Here, $x_0 = x(\tau = 0)$, $u_{x0} = u_x(\tau = 0)$, $s_0 = s(\tau = 0)$, $J_{00} = J_0(\tau = 0)$, $J_{10} = J_1(\tau = 0)$, $Y_{00} = Y_0(\tau = 0)$, $Y_{10} = Y_1(\tau = 0)$, and $W_0 = W(\tau = 0)$ are the initial conditions, and $W(s)$ is the Wronskian of $J_0(s)$ and $Y_0(s)$,

$$W(s) = \begin{vmatrix} -Y_1(s) & -Y_0(s) \\ J_1(s) & J_0(s) \end{vmatrix}.$$

The dependence of the maximum oscillation amplitude on the parameters μ_0 and ξ_0 during the electron propagation in the wakefield for a time $\tau = 4000$ is shown in Fig. 2 and

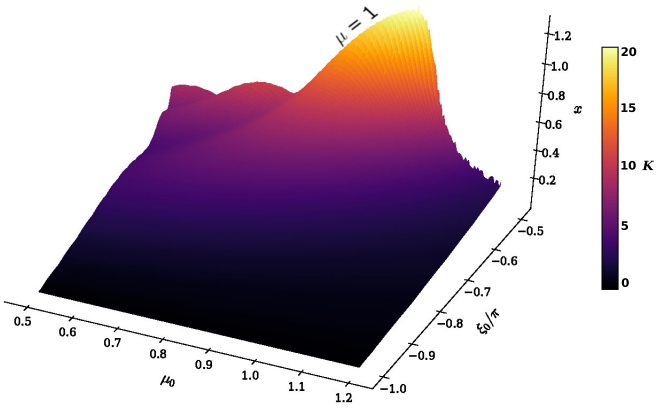

FIG. 2. The dependence of the maximum oscillation amplitude on the initial conditions μ_0 and ξ_0 from analytical solution $x(s)$. Color is scaled by the value of the strength parameter K.

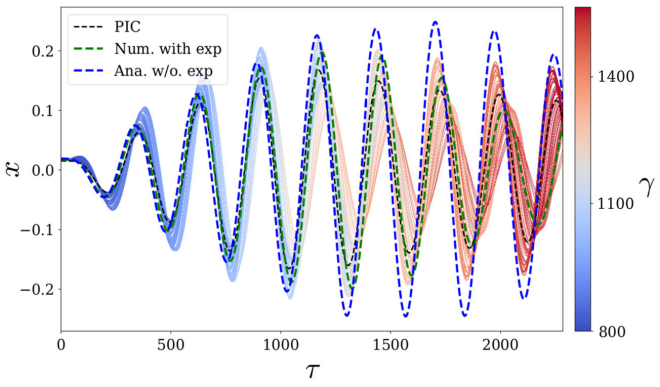

FIG. 3. Solid lines: Trajectories of electrons from 2D PIC simulation. The color map indicates the gamma factor of electrons. Dashed black line: The trajectory of one electron from PIC simulation. Dashed blue line: The trajectory of an electron given by the analytical solution in Eq. (7). Dashed green line: The trajectory of an electron given by the numerical solution of an electron by considering the exponential term in Eqs. (4) and (3).

the color is scaled by the parameter of maximum oscillation strength of the electron, K, which is also the maximum transverse momentum of the electron normalized with $m_e c$. It reaches the peak at its primary resonant state as seen at the ridge of the surface, where $\mu = -\mu_0/\sin\xi_0 = 1$, where the betatron oscillation of the electron is resonant with the laser centroid oscillation. On the other hand, this resonance can die out when $\mu \neq 1$. This can be achieved by the energy gain or loss of the electron, as indicated by the $R_\delta\tau$ term in Eq. (5). For the typical laser-plasma and electron beam configurations, R_δ is very small. For example, in our case $R_\delta \sim 10^{-4}$. It leads to a relatively long resonant process duration $\Delta\tau$, which is determined by the acceleration phase of the electron in the wakefield, $\Delta\tau \propto 1/|\xi_0 + \pi/2|$. As a result, the initial resonant process can persist for the time of a few oscillation periods sufficient to increase the oscillation amplitude. A semisteady oscillating pattern with a large amplitude will be formed subsequently after the resonance is totally broken where μ is far away from 1. It should be mentioned that the initial injection phase $\xi_0 = -\pi/2$ should be avoided because there is no acceleration at this injection phase, and then the resonance is undamped. This leads to continuous growth of the electron transverse amplitude till the electron escapes from the plasma wakefield transversely and is, hence, lost.

The analytical solution of $x(s)$ for $\mu = 1$ at $\xi_0 = -1.25\pi/2$ is plotted by the dashed blue line in Fig. 3. It is shown that the oscillation amplitude is increased during the initial resonance stage when $\tau < 1500$. After that, the oscillation remains semisteady when the electron is sufficiently accelerated to $\gamma > 1300$. The exponential term in the wakefield equations (3) and (4) decreases the oscillating amplitude and frequency, as seen by comparing the dashed blue and green lines in Fig. 3, but keeps the general behavior unchanged. Therefore, it is better to initially keep x_{c0}/w_m small to avoid a strong effect from the exponential term. However, a stronger K requires a larger initial centroid displacement of the laser pulse, since $g(s) \propto x_{c0}$, which limits the further extension of the radiation spectrum to a higher-energy region. For this purpose, nonlinear plasma wakefield should be considered, which will be discussed later.

The time evolution of the transverse size of a electron beam is governed by

$$\frac{d^2\sigma_x}{d\tau^2} - \frac{R_\delta}{1+R_\delta\tau}\frac{d\sigma_x}{d\tau} + \frac{\Omega^2}{\mu(1+R_\delta\tau)}\sigma_x - \frac{\varepsilon_x^2}{\sigma_x^3} = 0, \quad (8)$$

where $\sigma_x = \sqrt{\langle x^2\rangle - \langle x\rangle^2}$ is the transverse beam size in the $\hat{x}\,\hat{z}$ plane. Since the energy gain is very slow, $R_\delta \ll 1$, the energy gain in the early interaction stage can be neglected. The beam size remains approximately constant when the initial beam size is matched as $\sigma_{b,x,m} = \sqrt{\mu\varepsilon_{n,x}/(\gamma_0\Omega)}$, where $\varepsilon_{n,x}$ is the dimensionless normalized rms beam emittance. Thus, the beam divergence is given as $\sigma_{\theta,x,m} = \varepsilon_{n,x}/\sigma_{b,x,m}$. By matching such conditions, the dynamics of an electron beam with a moderate transverse beam size can also be described by Eq. (5) in the same way as a single electron. As shown in Fig. 3, the trajectories of an electron beam (solid lines) from a particle-in-cell (PIC) simulation agree well with the analytical solution of a single electron (blue dashed line).

2D particle-in-cell simulations have been performed for the initially resonant case with the 2D/3D PIC code LAPINE [23] on JURECA [24] at the Jülich Supercomputing Center. The resonant condition $\mu = 1$ is matched at the phase $\xi_0 = -1.25\pi/2$. An x-polarized Gaussian laser pulse with a wavelength of 1 μm propagates into a parabolic plasma channel with an offset $x_{c0} = 0.05$ with respect to the z axis. The normalized laser intensity is $a_0 = 0.9$ with a spot size of $w_0 = 1.6$ and a pulse duration FWHM (full width at half maximum) of $w_\tau = 10.2$. The initial on-axis plasma density along the propagation axis z is $n_{0,i} = 0.001 n_c$, where n_c is the laser critical density. The longitudinal plasma density

gradient is used to lock the injected electrons in the initial phase [22]. An electron beam with a Gaussian transverse profile $n_b(x) = n_{b0}\exp(-x^2/2\sigma_x^2)$ with $n_{b0} = 0.01n_{0,i}$ and $\sigma_x = 0.1$, corresponding to normalized emittance $\varepsilon_{n,x} = 0.0047$, is injected into the plasma channel. The beam profile in the longitudinal direction is uniform. The length of the beam is 1.8 μm, spanning over the phase range $-\pi < \xi_0 < -\pi/2$. The rms energy spread of the electron beam is $\sigma_\gamma/\gamma_0 = 1\%$ with $\gamma_0 = 800$. Such an electron beam can be obtained from a laser wakefield accelerator [25]. Trajectories of the electrons near the phase $\xi_0 = -1.25\pi/2$ inside the beam are shown by the solid lines in Fig. 3, and the color is scaled by the rms Lorentz factor of these selected electrons. The dashed black line is for the trajectory of the electron initially residing in the matched phase $\xi_0 = -1.25\pi/2$. An analytical solution of Eq. (7) for an electron with an initial phase $\xi_0 = -1.25\pi/2$ is presented by the green dashed line. It shows that the electron dynamics is weakly dependent on ξ_0, especially during the resonant stage $\tau < 1500$ due to the small energy gain rate R_δ. Therefore, the initial resonant process can be used to efficiently enhance the oscillation amplitude of the electron beam without severely increasing the beam divergence. The resonance dies out after $\tau > 1500$, where $\gamma > 1200$. The significant effect of the plasma density gradient can be seen after $\tau > 1800$ in Fig. 3, where the oscillation frequency of an electron in PIC simulation is higher than that from analytical calculation, by comparing the dashed black and green lines.

The radiation is calculated from the Lienard-Wiechert potentials [26]. The critical frequency is approximately given by $\omega_c = 3\gamma^3\Omega x_a/2$, with x_a being the maximum amplitude of transverse electron oscillation. For a Gaussian laser pulse, the critical frequency is then estimated as $\omega_c \simeq (-6\gamma^2 a_0^2 C x_a \sin\xi_0)/w_m^2$. By using the averaged value of the Lorentz factor of the electron beam, $\gamma_{\mathrm{ave}} \simeq 1150$, after it propagates $\tau = 2500$ in the plasma wakefield, the peak frequency of the on-axis radiation is then estimated as $\omega_{\mathrm{peak}} = 0.3\omega_c \simeq 0.12$ MeV, which agrees with the numerical calculation in Fig. 4. It is calculated with the trajectory from the VDSR [27] simulation shown by the dashed green line in Fig. 3, where $K \simeq 15$. The peak brightness is $10^{20}\,\mathrm{ph/s/mm^2/mrad^2/0.1\%bandwidth(BW)}$ with a photon energy between 50 and 150 keV, which is comparable to the typical third-generation light sources [28]. For a nonresonant case with comparable parameters, the spectrum peaks at 1 keV [15], which is 2 orders of magnitude lower than the resonant case.

Higher critical frequency requires a larger x_a and then a larger initial laser pulse displacement x_{c0}. For a fixed spot size of laser pulse w_m, the increase of x_a is limited by the exponential term in the linear wakefield, as seen in Eqs. (3) and (4). As a result, it is impossible to limitlessly increase the radiation spectrum to higher energy ranges. For the linear case, the energy of the emitted photon is limited to less than 1 MeV. However, a nonlinear laser-plasma wakefield can be considered to further increase the energy $\hbar\omega_c > 1$ MeV. A 2D PIC simulation for the nonlinear case has also been preformed with a laser pulse of $a_0 = 3.0$ and $x'_{c0} = 1.5$ μm. The generated plasma bubble can still oscillate, and it is possible to drive the self-trapped electrons into the resonant betatron motion. The on-axis radiation spectrum is extended, as shown by the blue line in Fig. 4, and the peak is around 2 MeV. Our scheme potentially provides about 2 orders of magnitude higher photon energies than the betatron radiation generated directly from the plasma bubble [9,29], and about 1 order of magnitude higher energies than the recently proposed plasma-based gamma-ray source [2].

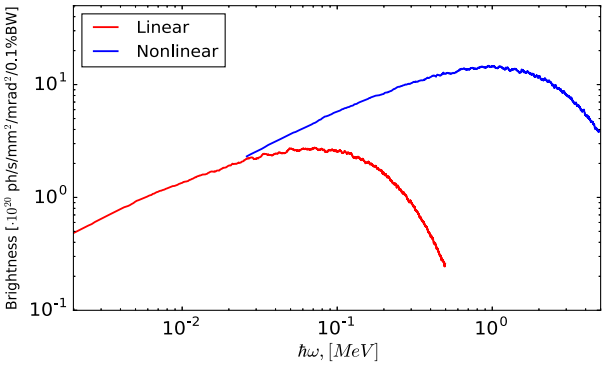

FIG. 4. On-axis radiation spectrum in the plasma-wakefield wiggler. Red: Linear case. Blue: Nonlinear case.

In conclusion, a compact laser-plasma-based wiggler is proposed to generate gamma rays. Such a wiggler is able to work in the linear laser-plasma wakefield regime, in which the electron oscillation amplitude is enhanced by the resonance of betatron oscillation and centroid oscillation. The limitation of the linear wakefield can be overcome by considering the nonlinear regime, in which case the self-trapped electrons are resonantly oscillated and the energy of emitted photons can be further enhanced to the strong gamma-ray range with a higher brightness. This flexible and compact scheme may provide a wide range of applications in scientific research, medicine, and industry.

This work was supported by the Helmholtz Association (Helmholtz Young Investigators group VH-NG-1037) and in part by by NSFC (11674341). The authors gratefully acknowledge the computing time granted by the John von Neumann Institute for Computing (NIC) and provided on the supercomputer JURECA at the Jülich Supercomputing Center (JSC).

*B.Lei@gsi.de
†J.Wang@gsi.de
‡S.Rykovanov@gsi.de

[1] A. A. Kordbacheh, B. Maraghechi, B. Farokhi, and J. E. Willett, Phys. Plasmas **12**, 113106 (2005).
[2] S. Cipiccia *et al.*, Nat. Phys. **7**, 867 (2011).

[3] S. Kneip *et al.*, Nat. Phys. **6**, 980 (2010).
[4] A. Rousse, C. Rischel, and J.-C. Gauthier, Rev. Mod. Phys. **73**, 17 (2001).
[5] C. DesRosiers, V. Moskvin, A. F. Bielajew, and L. Papiez, Phys. Med. Biol. **45**, 1781 (2000).
[6] B. Brozek-Pluska, D. Gliger, A. Hallou, V. Malka, and Y. A. Gauduel, Radiat. Phys. Chem. **72**, 149 (2005).
[7] B. Grosswendt, Radiation Protection Dosimetry **115**, 1 (2005).
[8] S. Kiselev, A. Pukhov, and I. Kostyukov, Phys. Rev. Lett. **93**, 135004 (2004).
[9] A. Rousse, K. T. Phuoc, R. Shah, A. Pukhov, E. Lefebvre, V. Malka, S. Kiselev, F. Burgy, J.-P. Rousseau, D. Umstadter, and D. Hulin, Phys. Rev. Lett. **93**, 135005 (2004).
[10] M. Chen, J. Luo, F.-Y. Li, F. Liu, Z.-M. Sheng, and J. Zhang, Light Sci. Appl. **5**, e16015 (2016).
[11] S. P. D. Mangles, A. G. R. Thomas, M. C. Kaluza, O. Lundh, F. Lindau, A. Persson, F. S. Tsung, Z. Najmudin, W. B. Mori, C.-G. Wahlström, and K. Krushelnick, Phys. Rev. Lett. **96**, 215001 (2006).
[12] K. Németh, B. Shen, Y. Li, H. Shang, R. Crowell, K. C. Harkay, and J. R. Cary, Phys. Rev. Lett. **100**, 095002 (2008).
[13] Y. Ma, L. Chen, D. Li, W. Yan, K. Huang, M. Chen, Z. Sheng, K. Nakajima, T. Tajima, and J. Zhang, Sci. Rep. **6**, 30491 (2016).
[14] S. G. Rykovanov, C. B. Schroeder, E. Esarey, C. G. R. Geddes, and W. P. Leemans, Phys. Rev. Lett. **114**, 145003 (2015).
[15] S. G. Rykovanov, J. W. Wang, V. Y. Kharin, B. Lei, C. B. Schroeder, C. G. R. Geddes, E. Esarey, and W. P. Leemans, Phys. Rev. ST Accel. Beams **19**, 090703 (2016).
[16] J. W. Wang, C. B. Schroeder, R. Li, M. Zepf, and S. G. Rykovanov, Sci. Rep. **7**, 16884 (2017).
[17] C. G. R. Geddes, C. Toth, J. van Tilborg, E. Esarey, C. B. Schroeder, J. Cary, and W. P. Leemans, Phys. Rev. Lett. **95**, 145002 (2005).
[18] Y. F. Li *et al.*, Phys. Plasmas **24**, 023108 (2017).
[19] W. P. Leemans, A. J. Gonsalves, H.-S. Mao, K. Nakamura, C. Benedetti, C. B. Schroeder, C. Tóth, J. Daniels, D. E. Mittelberger, S. S. Bulanov, J.-L. Vay, C. G. R. Geddes, and E. Esarey, Phys. Rev. Lett. **113**, 245002 (2014).
[20] P. Sprangle, J. Krall, and E. Esarey, Phys. Rev. Lett. **73**, 3544 (1994).
[21] E. Esarey, C. B. Schroeder, and W. P. Leemans, Rev. Mod. Phys. **81**, 1229 (2009).
[22] W. Rittershofer, C. B. Schroeder, E. Esarey, F. J. Grüner, and W. P. Leemans, Phys. Plasmas **17**, 063104 (2010).
[23] H. Xu, W. Chang, H. Zhuo, L. Cao, and Z. Yue, Chin. J. Comput. Phys. **19**, 305 (2002); http://en.cnki.com.cn/Article_en/CJFDTotal-JSWL200204004.htm.
[24] D. Krause and P. Thörnig, J. Large-Scale Res. Facil. **2**, A62 (2016).
[25] W. T. Wang, W. T. Li, J. S. Liu, Z. J. Zhang, R. Qi, C. H. Yu, J. Q. Liu, M. Fang, Z. Y. Qin, C. Wang, Y. Xu, F. X. Wu, Y. X. Leng, R. X. Li, and Z. Z. Xu, Phys. Rev. Lett. **117**, 124801 (2016).
[26] J. Jackson, *Classical Electrodynamics*, 3rd ed. (Wiley, New York, 1999).
[27] M. Chen, E. Esarey, C. G. R. Geddes, C. B. Schroeder, G. R. Plateau, S. S. Bulanov, S. Rykovanov, and W. P. Leemans, Phys. Rev. ST Accel. Beams **16**, 030701 (2013).
[28] DESY, Petra III: Facility information, http://photon-science.desy.de/facilities/petra_iii/facility_information/index_eng.html, 2017.
[29] S. Kneip *et al.*, Phys. Rev. Lett. **100**, 105006 (2008).